Exploring cluster formation in Zr-MOF synthesis in situ with X-ray absorption spectroscopy

Olena Zavorotynska,[1,] Anna Cecilie Åsland,[1] Pascal D. C. Dietzel,[2] and Sachin M. Chavan [3,*]*

[1] Department of Mathematics and Physics, University of Stavanger, Stavanger P.O. Box 8600, NO-4036 Forus, Norway.

[2] Department of Chemistry, University of Bergen, P.O. Box 7803, N-5020 Bergen, Norway.

[3] Department of Chemistry, Bioscience and Environmental Engineering, University of Stavanger, Stavanger P.O. Box 8600, NO-4036 Forus, Norway.

Electronic Supplementary Information

Content

1. Synthesis

Table S1. Reagents stoichiometries in the synthesis reactions.

N	$ZrCl_4$ (g)	Fumaric acid (g) (FA)	Water (ml)	Acetic acid (ml) (MOD)	DMF (ml)	Temp. (°C)	Reaction time (min)	Stoichiometry, eq. ($ZrCl_4$:FA:H_2O: MOD:DMF)
$ZrCl_4$-DMF solution								
r1	0.255	0	0	0	4.0	120	97	1:0:0:0:49
r2	0.250	0	0.058	1.23	4.0	120	44	1:0:3:20:49
Zr-fumerate synthesis reactions								
r3	0.250	0.374	0	0	4.0	120	143	1:3:0:0:49
r4	0.250	0.374	0	0.613	4.0	120	171	1:3:0:10:49
r5	0.250	0.374	0.058	0	4.0	120	67	1:3:3:0:49
r6	0.250	0.374	0.058	0.613	4.0	120	257	1:3:3:10:49
r7	0.250	0.374	0.058	1.23	4.0	120	77	1:3:3:20:49
r8	0.250	0.374	0.155	1.23	4.0	120	55	1:3:8:20:49
r9	0.250	0.374	0.058	1.23	4.0	100	55	1:3:3:20:49
r10	0.250	0.374	0.058	1.23	4.0	130	49	1:3:3:20:49

2. XAS spectra of reference compounds

i)

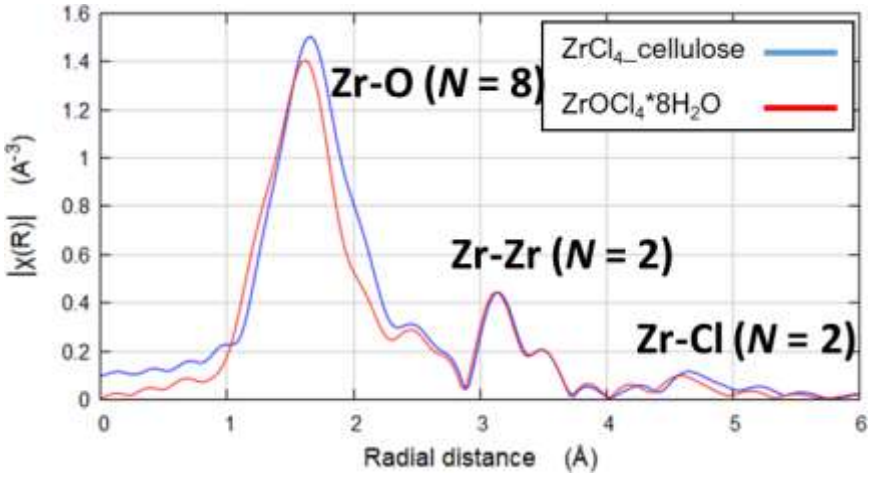

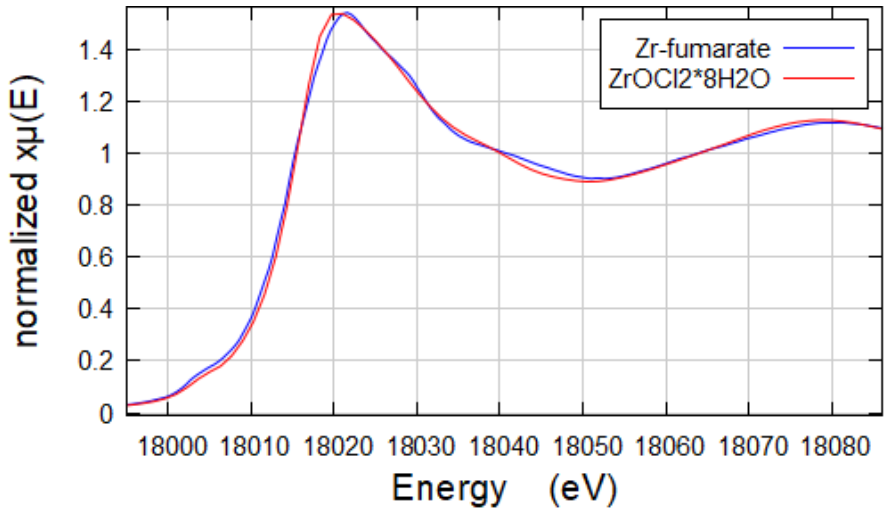

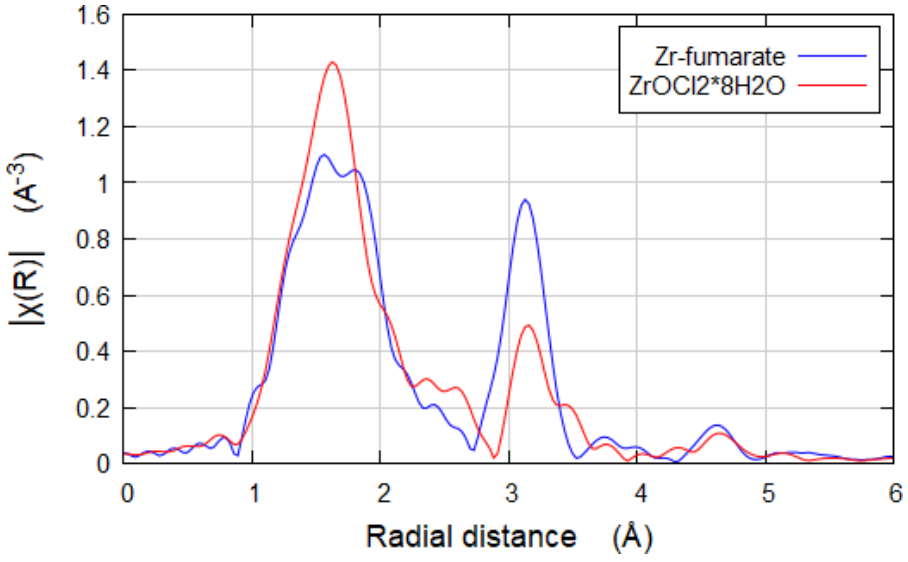

ii)

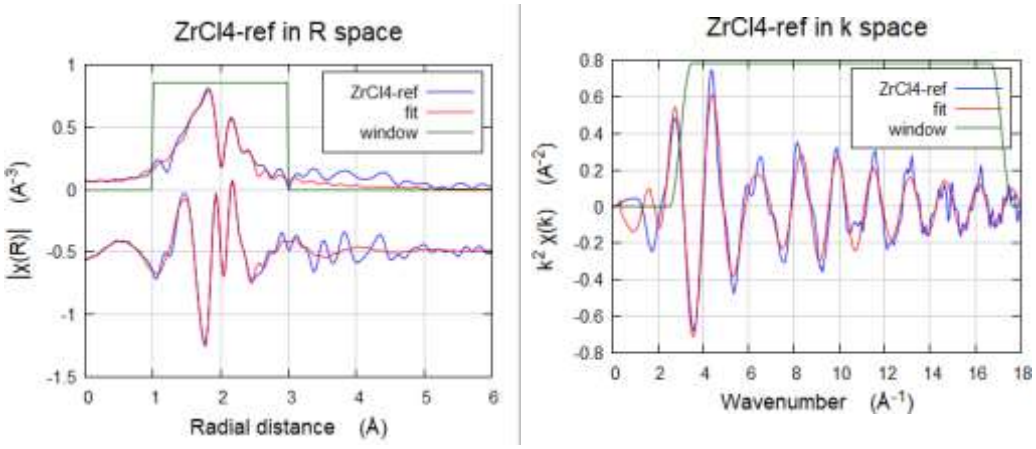

k-range used for FT	3.000 – 17.181
k-weight	1, 2, 3
R-factor by *k*-weight	1 -> 0.00655, 2 -> 0.01837, 3 -> 0.0452323
N_{ind}	17.6
N_{var}	8
χ^2	7263
χ^2	754
ΔE_0	0.6 ± 0.6 eV
Amplitude, S_0^2	0.83 ± 0.06

Shell	*R* (Å)	*N*	σ^2 (Å^2) [a]
Zr-Cl1	2.318(6)	2	0.0020(5)
Zr-Cl2	2.490(12)	2	0.004(1)
Zr-Cl3	2.637(14)	2	0.006(2)

Fig. S1a i) Experimental spectra of $ZrCl_4$, $ZrOCl_2$*($8H_2O$), and Zr-fumarate as cellulose-supported pellets. The peaks are assigned based on the calculation of the cluster geometry[1] by ATOMS.[2] ii) Fit results of the reference anhydrous $ZrCl_4$-ref.

3. EXAFS fitting and LCF details of r1-r2

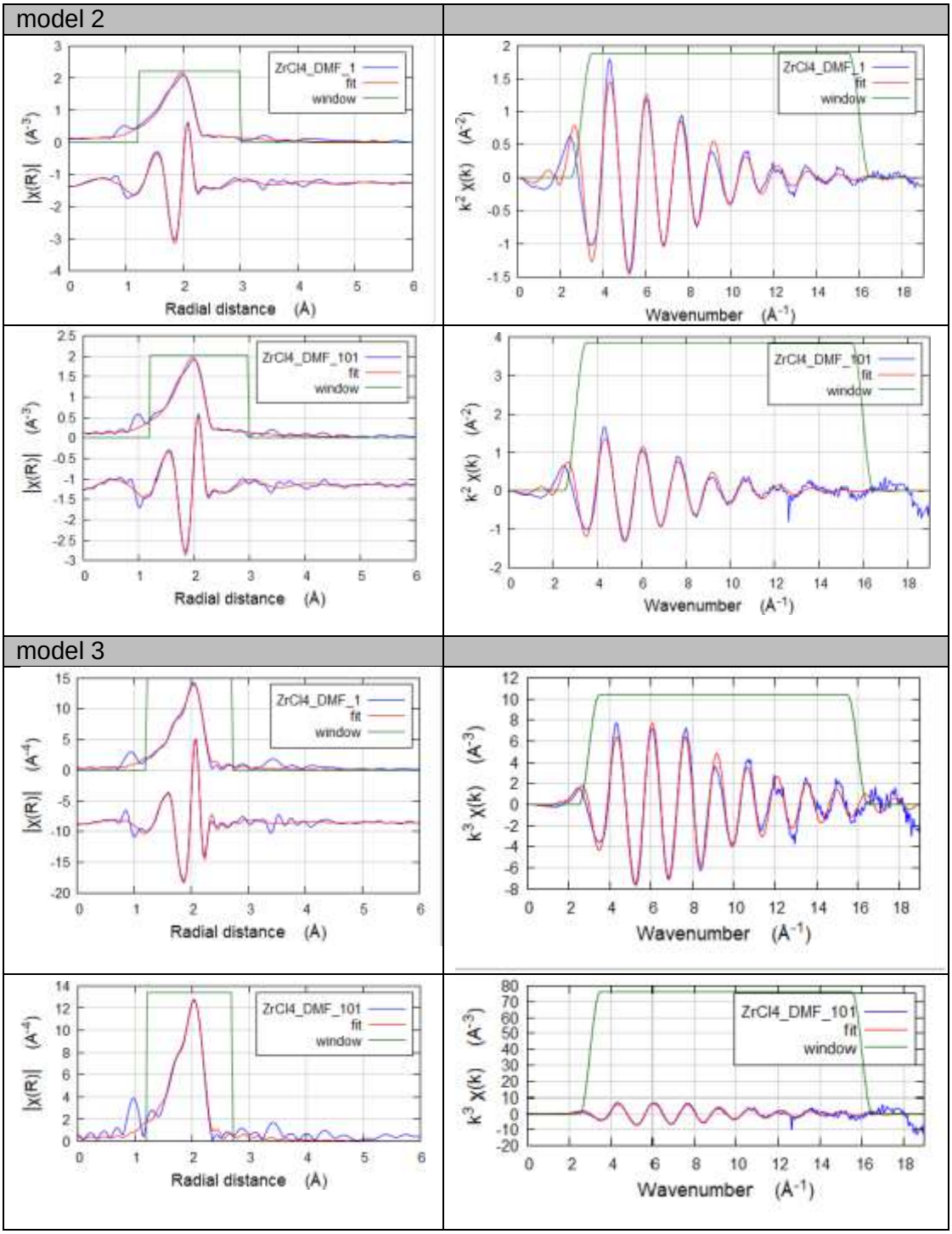

Fig. S1b Zr k-edge EXAFS *R*-space fit results for $ZrCl_4$-DMF solution, first and last spectra in the series. FT of magnitude of EXAFS data (blue line), and corresponding fit (red line) are shown, as well as the real part of the FT data and the corresponding fits. Fitting region is indicated by green box. See Table 2 for fit parameters and results. EXAFS function in k <= 18 $Å^{-1}$ range is also shown.

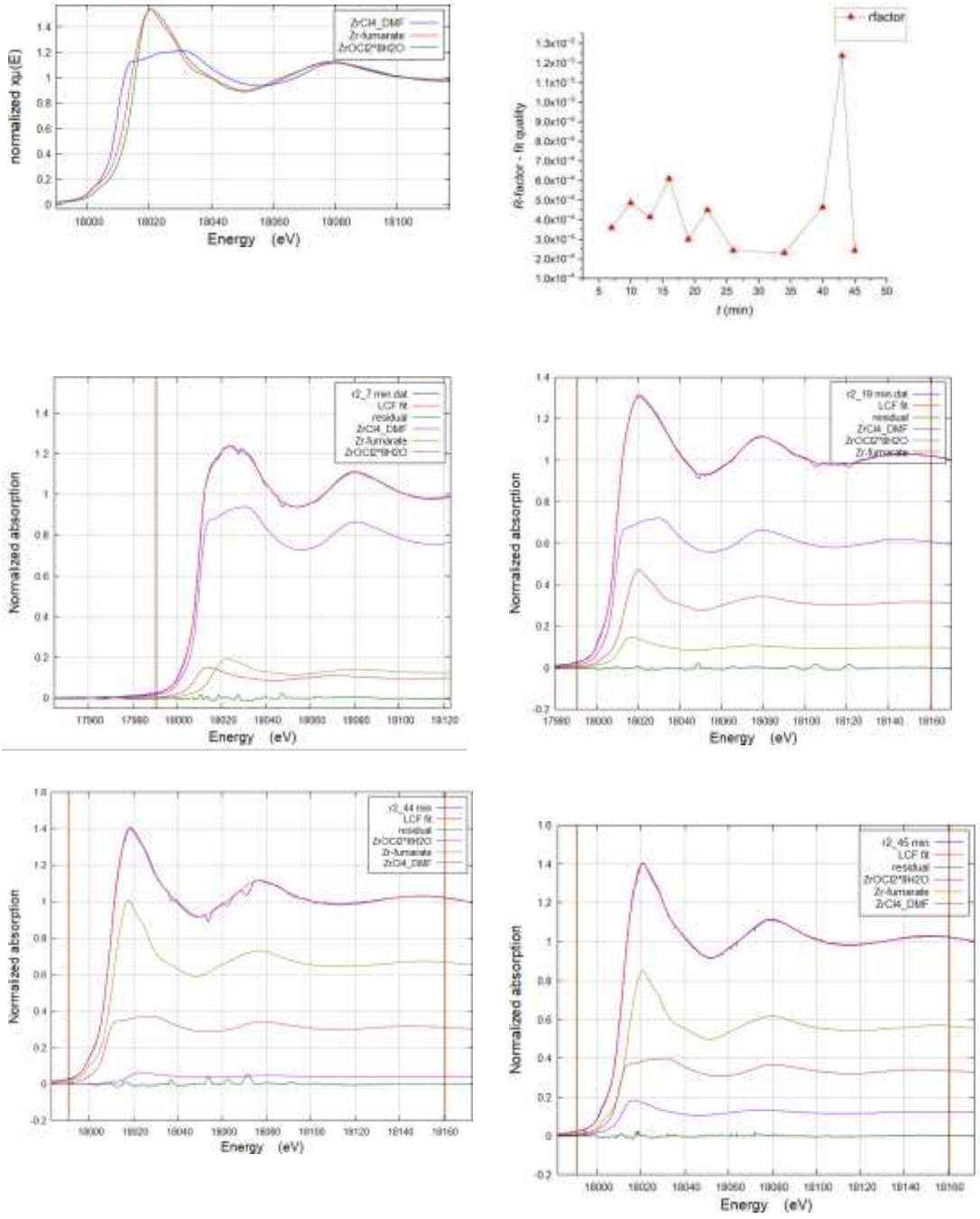

Fig. S1c The three references used for LCF, *R*-factor of the fits, and the representative examples of the fits for the $ZrCl_4$-H_2O-MOD-DMF solution (r2), for the data presented in the Figure 2c. The references and the standards were aligned to Zr reference foil standard before the fitting.

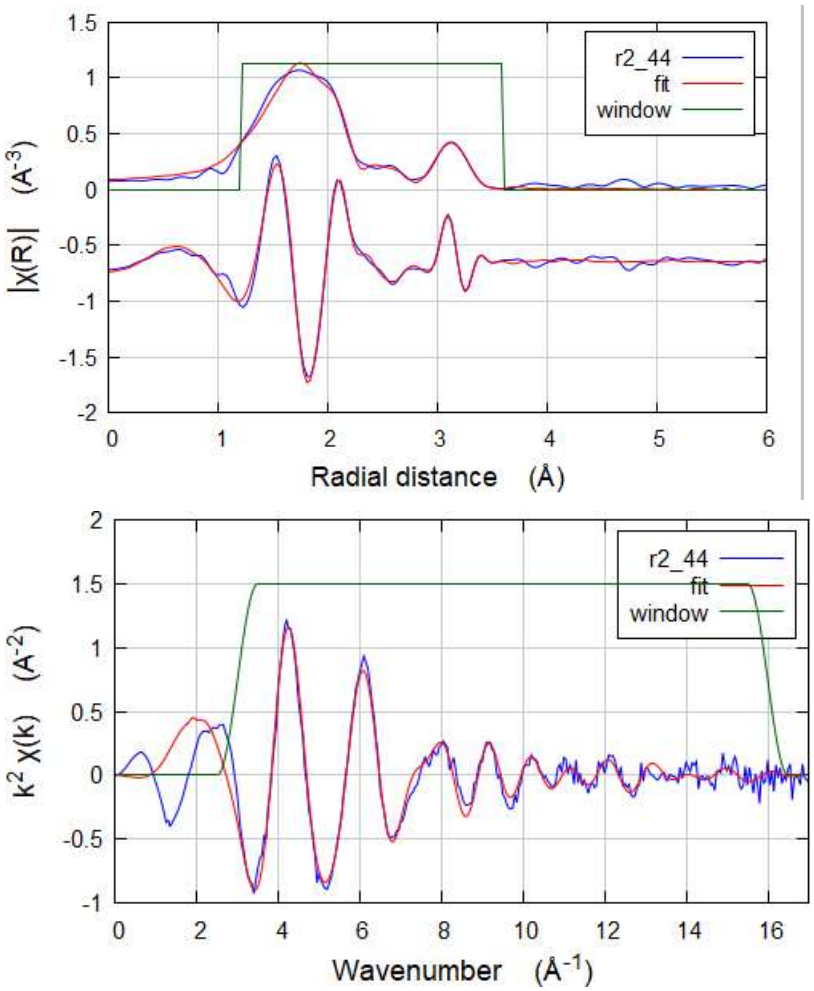

Fig. S1d Zr k-edge EXAFS *R*-space fit results for the final spectrum of $ZrCl_4$-DMF-H_2O-MOD solution (merged spectra at 43-45 min, r2_44 in the Table 2). FT of magnitude of the EXAFS data (blue line), and corresponding fit (red line) are shown, as well as the real part of the FT data and the corresponding fits. Fitting region is indicated by green box. The contributions from the single scattering paths used in the fit are also shown. See Table 2 for fit parameters and results. EXAFS function in k <= 18 $Å^{-1}$ range is also shown.

4. MOF synthesis reactions

4.1 LCF of r3-r6 reactions

r3

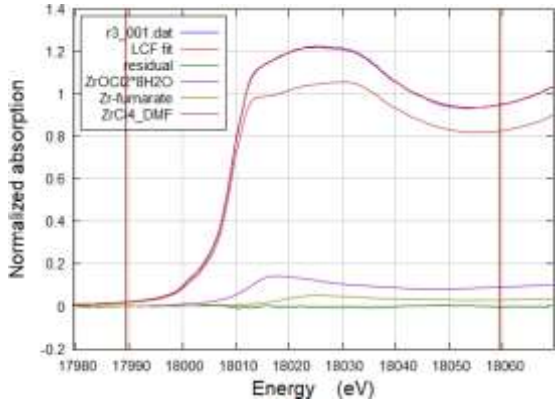

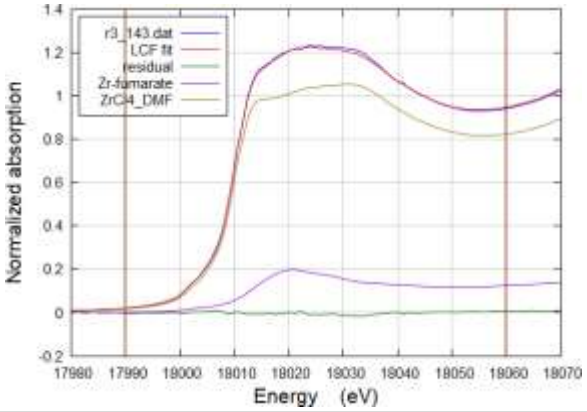

r4

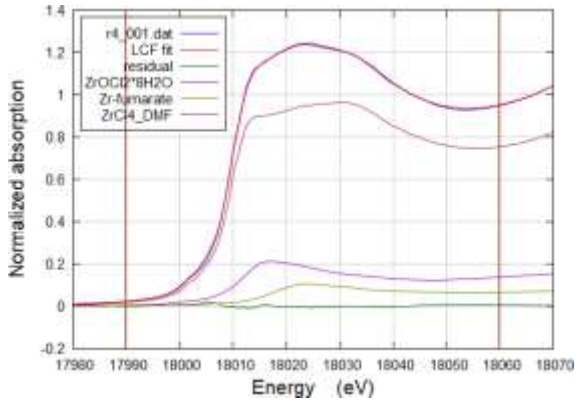

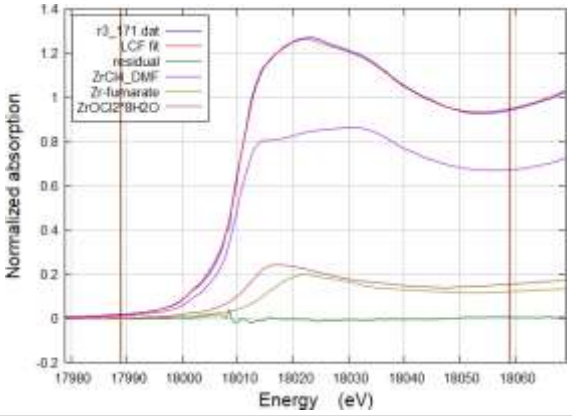

r5

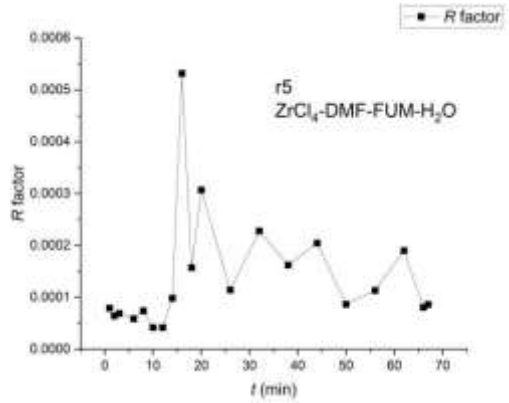

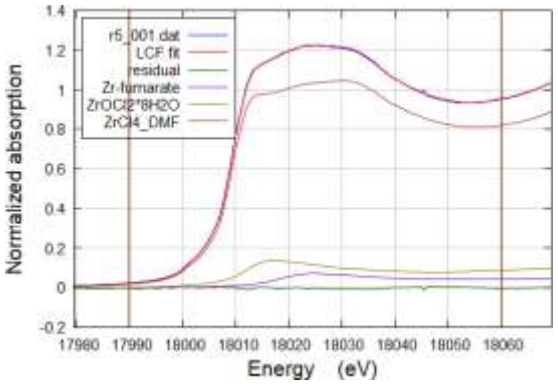

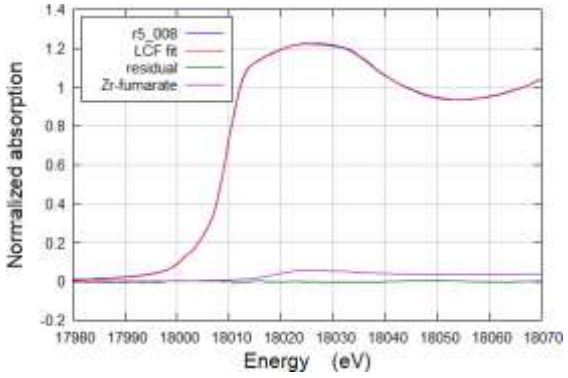
r5_008
LCF fit
residual
Zr-fumarate
Normalized absorption
Energy (eV)

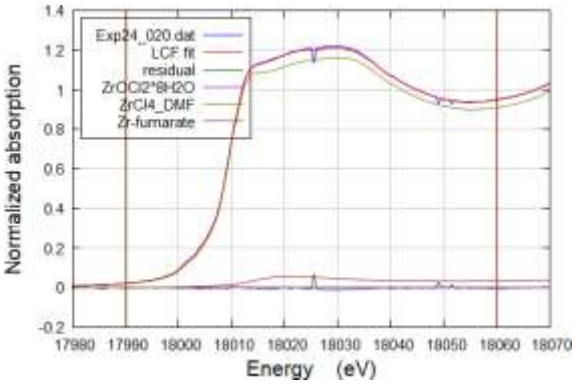
Exp24_020.dat
LCF fit
residual
ZrOCl2*8H2O
ZrCl4_DMF
Zr-fumarate
Normalized absorption
Energy (eV)

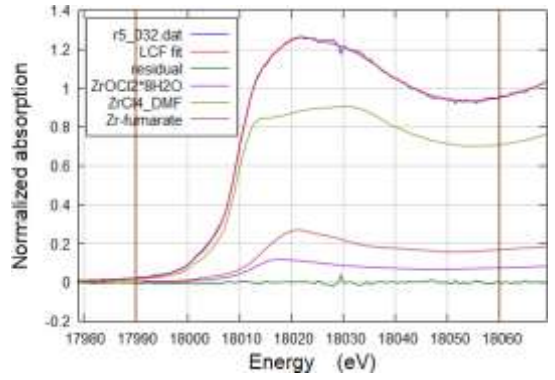
r5_032.dat
LCF fit
residual
ZrOCl2*8H2O
ZrCl4_DMF
Zr-fumarate
Normalized absorption
Energy (eV)

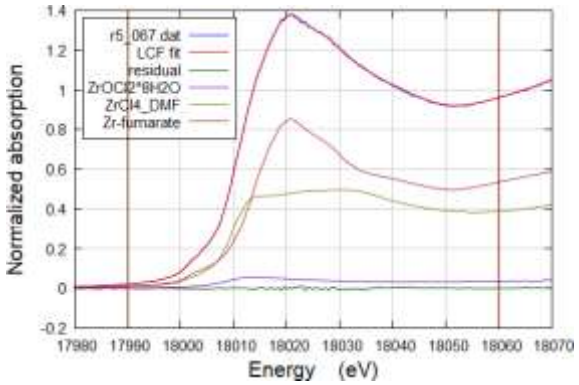
r5_067.dat
LCF fit
residual
ZrOCl2*8H2O
ZrCl4_DMF
Zr-fumarate
Normalized absorption
Energy (eV)

r6

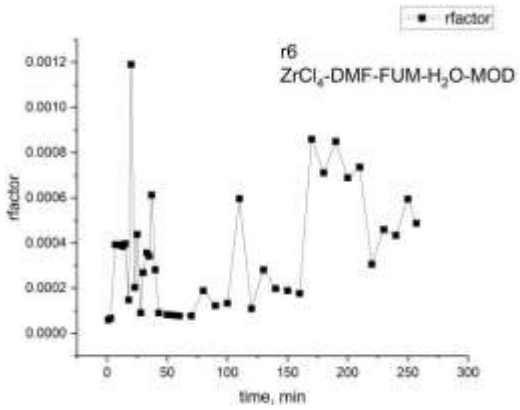
rfactor
r6
ZrCl4-DMF-FUM-H2O-MOD
rfactor
time, min

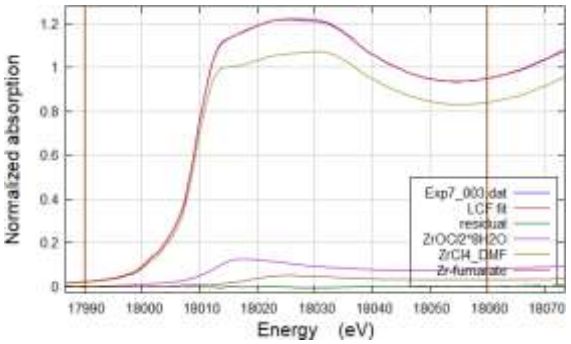
Exp7_003.dat
LCF fit
residual
ZrOCl2*8H2O
ZrCl4_DMF
Zr-fumarate
Normalized absorption
Energy (eV)

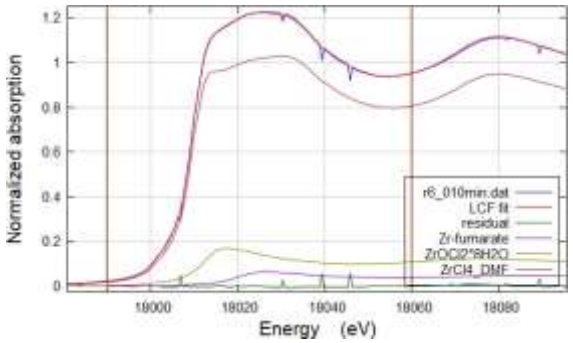
r6_010min.dat
LCF fit
residual
Zr-fumarate
ZrOCl2*8H2O
ZrCl4_DMF
Normalized absorption
Energy (eV)

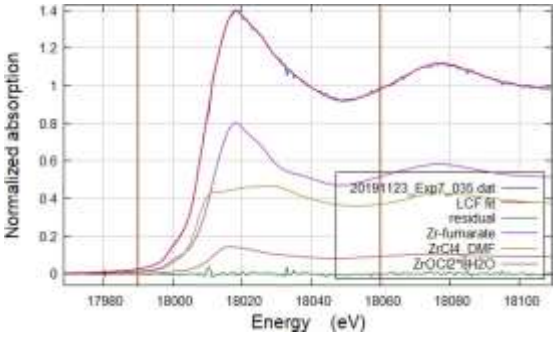
20191123_Exp7_030.dat
LCF fit
residual
Zr-fumarate
ZrCl4_DMF
ZrOCl2*8H2O
Normalized absorption
Energy (eV)

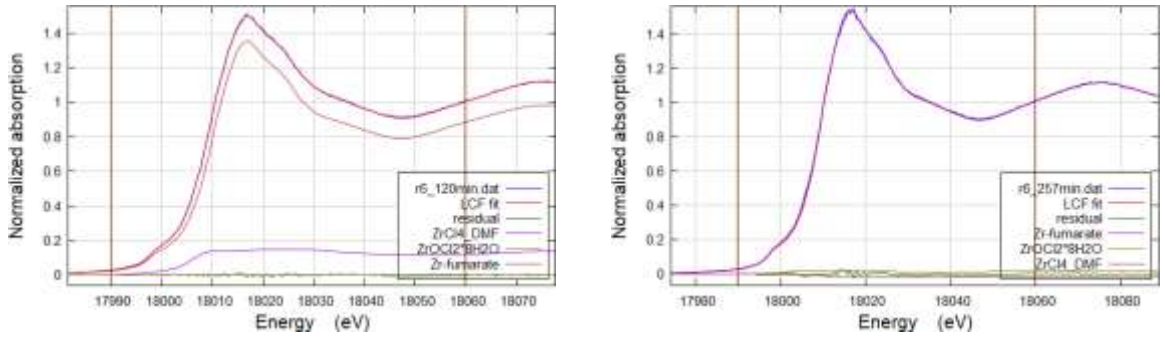

Fig. S2. Representative fits and *R*-factors of LCFs for r3-r6. The fits were performed with three references: $ZrCl_4$-DMF, Zr-fumarate (Zr-oxocluster), and $ZrOCl_2 \cdot 8H_2O$ (Zr-tetramer).

4.2 Local structure of Zr^{4+} in MOF-synthesis reaction with water and modulator (r6)

The final EXAFS spectrum obtained by merging last 4 spectra of the reaction was fitted to the MOF-801 cluster structure. The crystallographic data by Furukawa et al.[3] were used as an input for FEFF6 calculations in ARTEMIS software of the DEMETER XAS package. [2] In this structure, atom pairs O1-O3 and O2-O8 have partial occupancies 0.5. Thus, the atoms O3 and O2 were removed and the occupancies of the atoms O8 and O1 were increased to 1 in order for the structure to be processed by FEFF (Fig. S3). In the original structure, O3 share the occupancies with O1. The three Zr-O3 distances vary between 2.050 - 2.070 Å whereas those of O1 between 2.234 – 2.264 Å. One O2 share the occupancy with O8 atom, and the Zr-O distances are 2.256 and 2.065 Å, respectively. I.e., the atoms with the partial occupancies are accounted for by two

Table S2. Fit results of the EXAFS data for the 4 merged final spectra in the MOF synthesis with DMF with water and modulator: r6_252-256 min.

Model 1

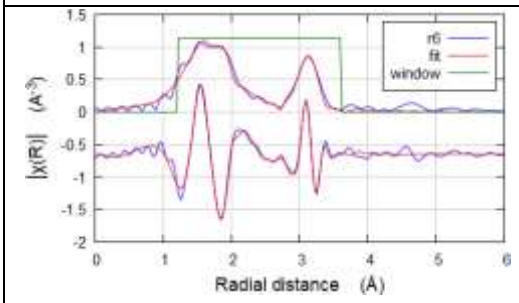

R-factor	0.018
N_{ind}	23
N_{var}	15
χ^2	2907
χ^2_ν	366
ΔE_0	- 4.8 ± 2.5 eV
Amplitude, S_0^2	1.6 ± 0.5

Shell	R_{input} (Å) [4]	R_{result} (Å)	N_{input} (not fitted)	Debye-Waller factor, σ^2 (Å
Zr – O8	2.065	2.052	1	- 0.003 ± 0.002
Zr – O4	2.239	2.220	6	0.009 ± 0.002
Zr – O1	2.264	1.870	1	0.020 ± 0.013
Zr – C1	3.211	3.422	4	0.018 ± 0.015
Zr – Zr	3.501	3.491	4	0.007 ± 0.002
Zr – O6	3.621	3.495	4	0.013 ± 0.025
Zr – O4 – C1 – O4	3.513	3.895	4	0.018 ± 0.015 (= σ^2 (C1))
Zr – O4 – C1	3.362	3.118	8	0.0216 ± 0.018 (= σ^2 (C1)

Model 2

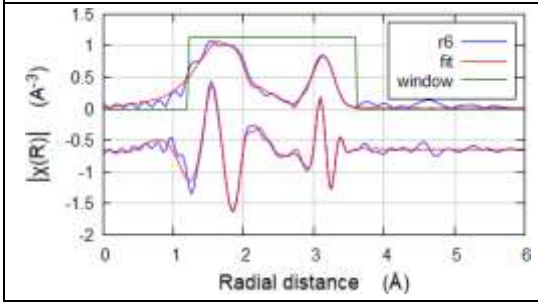

R-factor	0.020
N_{ind}	23
N_{var}	11
χ^2	5184
χ^2_ν	434
ΔE_0	- 2.7 ± 1.5 eV
Amplitude, S_0^2	1.12 ± 0.14

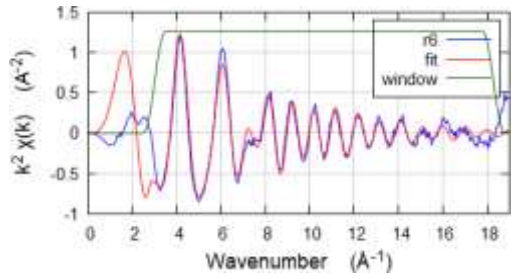

Shell	R_{input} (Å) [4]	R_{result} (Å)	N_{input} (not fitted)	Debye-Waller factor, σ^2 (Å^2)
Zr – O8	2.065	2.067	1	0.003 (set)
Zr – O4	2.239	2.214	6	0.008 ± 0.003
Zr – O1	2.264	2.308	1	0.003 (set)
Zr – C1	3.211	3.47	4	0.01 (set)
Zr – Zr	3.501	3.515	4	0.0053 ± 0.0007
Zr – O6.2	3.621	3.497	4	0.01 (set)
Zr – O4 – C1 – O4	3.513	3.986	4	0.01 (set)
Zr – O4 – C1	3.362	3.163	8	0.01 (set)

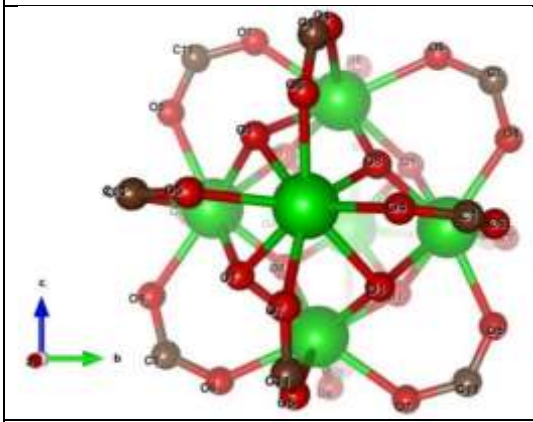

Fig S3. Cluster of Zr-fumarate[3] with edited occupancies as described in the text. Zr atoms are depicted in green, Oxygen – in red, Carbon – brown.

distinct single scattering paths with the average R_{eff} of 2.065 Å and 2.239 Å in each of the pairs. All these are bridging μ_3-O bonds. The remaining oxygen atoms are bonded to the carbon atoms of the linker with the bond distances between 2.228 – 2.242 Å, i.e. the relative paths are accounted for by the average R_{eff} of 2.239 Å. At least one path is accounted for by yet another R_{eff} of 2.264 Å (Zr-O1, also a μ_3-O bond). In this way, removing the atoms with partial occupancies will introduce significant alteration in the number of atoms in the coordination shells of the eight oxygens that is expected to result in a worse fit with larger disorder factors.

The $k^{0.5}$, k^1, k^2, and k^3-weighted data were fit simultaneously in 1.2 – 3.59 Å range (two coordination shells, k = 3.00 – 18.3 Å) in R-space. All the single scattering paths and those double-scattering paths with contribution rank above 10 % were included in the fits. Firstly, edge energy shift, ΔE_0, total amplitude, S_0^2, position of the atoms, and Debye-Waller factors, σ^2, were relaxed. Fit parameters and results are summarized in the Table S2 (Model 1). The fit to the model 1 is visually good and has a low R-value, however, the Debye-Waller parameters for the single and multiple scattering paths associated with O1 and O8 are negative and nearly negative, respectively, and Zr – O1 distance is unphysical indicating the problem with this model. Fixing the amplitude to the value of 0.81, obtained from the fit to Zr foil standard resulted in physical distances but almost all σ^2 were either negative or ill-defined. Among the various modifications of this model, the best results were obtained yet relaxing the amplitude but setting the troubling σ^2 factors to some reasonable values. The results are summarized in the table S2 under the *Model 2*. The most reasonable σ^2 values were obtained for the six oxygen atoms at R_{eff} of 2.239 Å and the Zr atoms responsible for the most intensity of the peak at 3.1 Å (R_{eff} = 3.501 Å). This result was characteristic for the vast majority of the fitting attempts (ca. 250) as well as the two reported here in the Table S2.

4.3 Kinetics series

r7

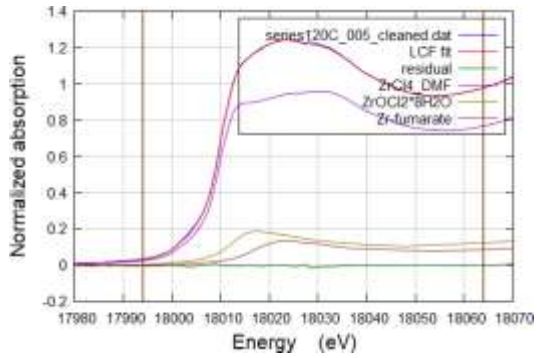

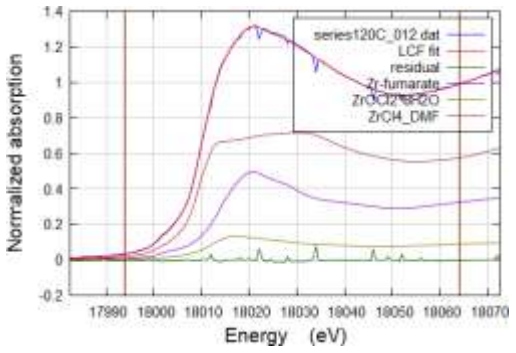

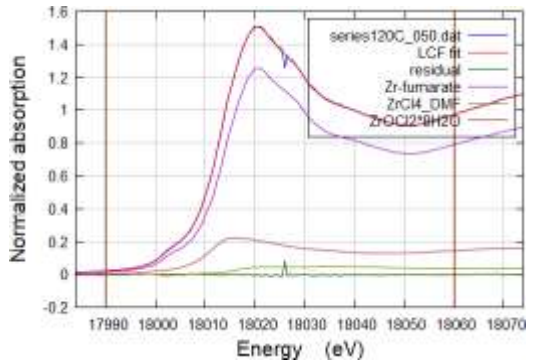

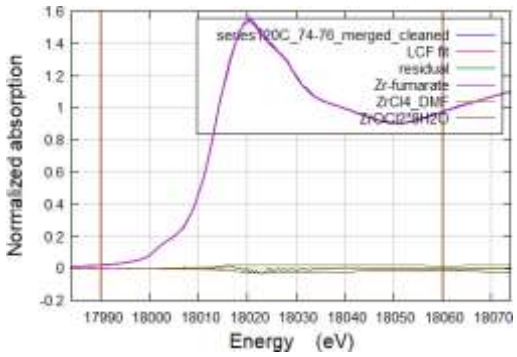

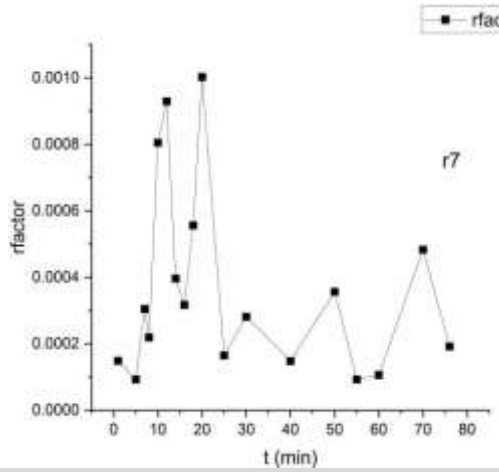

r8

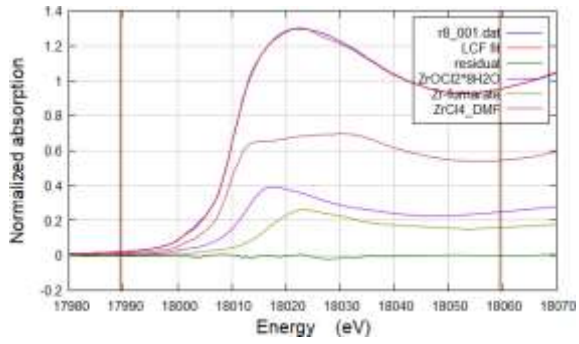

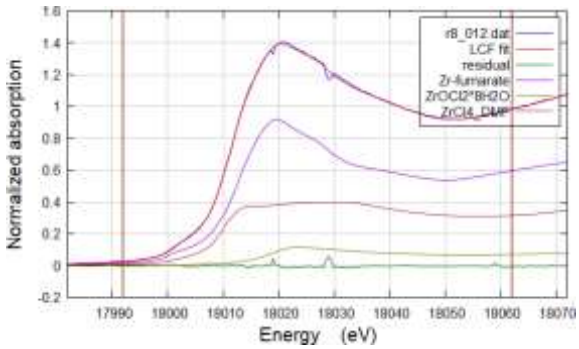

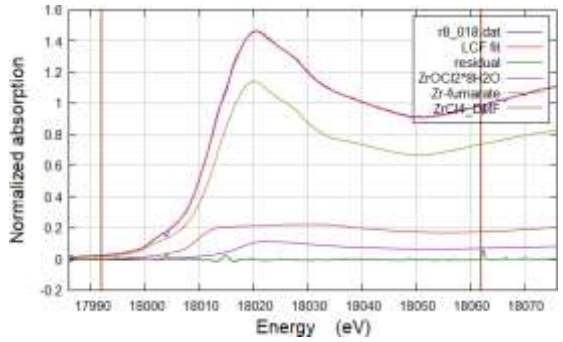
r8_018.dat
LCF fit
residual
ZrOCl2*8H2O
Zr-fumarate
ZrCl4_DMF
Normalized absorption
Energy (eV)

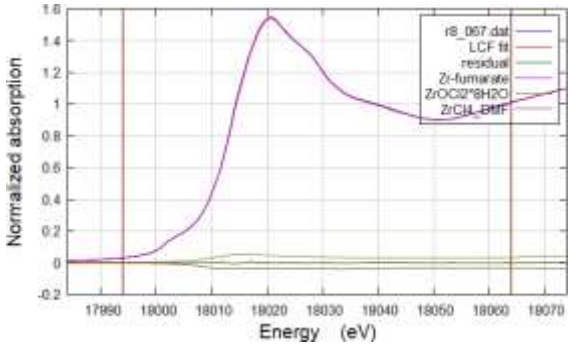
r8_067.dat
LCF fit
residual
Zr-fumarate
ZrOCl2*8H2O
ZrCl4_DMF
Normalized absorption
Energy (eV)

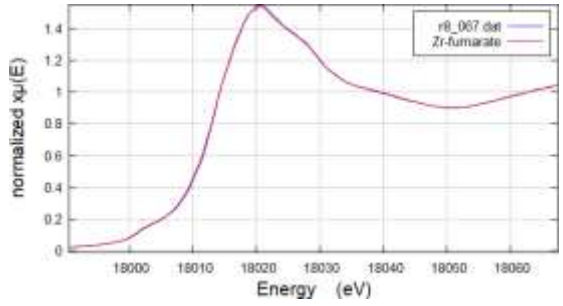
r8_067.dat
Zr-fumarate
normalized xμ(E)
Energy (eV)

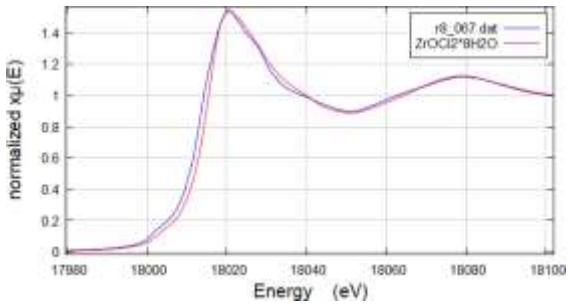
r8_067.dat
ZrOCl2*8H2O
normalized xμ(E)
Energy (eV)

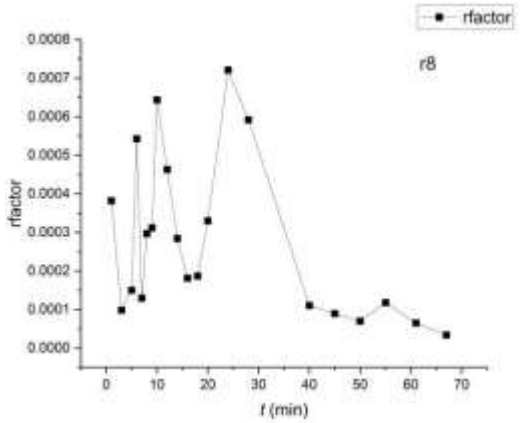
rfactor
r8
rfactor
t (min)

r9

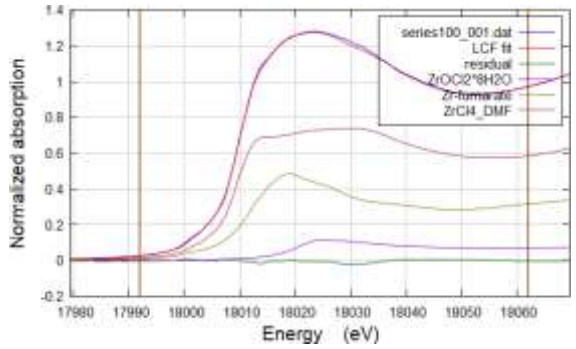
series100_001.dat
LCF fit
residual
ZrOCl2*8H2O
Zr-fumarate
ZrCl4_DMF
Normalized absorption
Energy (eV)

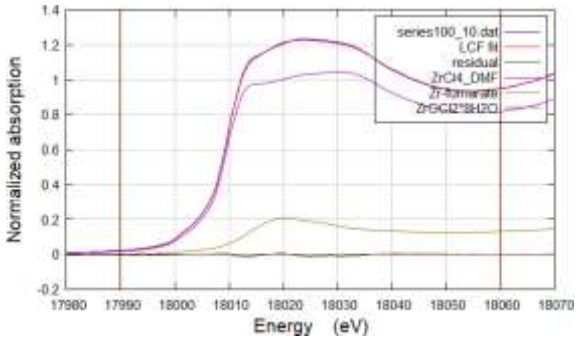
series100_10.dat
LCF fit
residual
ZrCl4_DMF
Zr-fumarate
ZrOCl2*8H2O
Normalized absorption
Energy (eV)

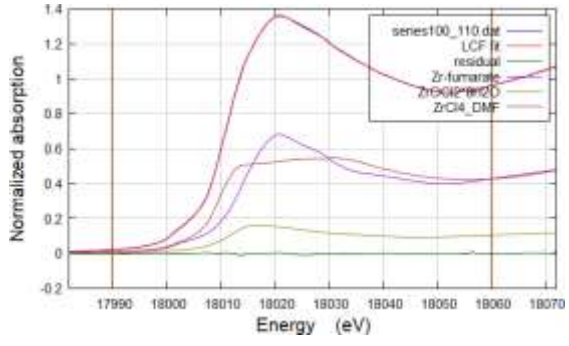
series100_110.dat
LCF fit
residual
Zr-fumarate
ZrOCl2*8H2O
ZrCl4_DMF
Normalized absorption
Energy (eV)

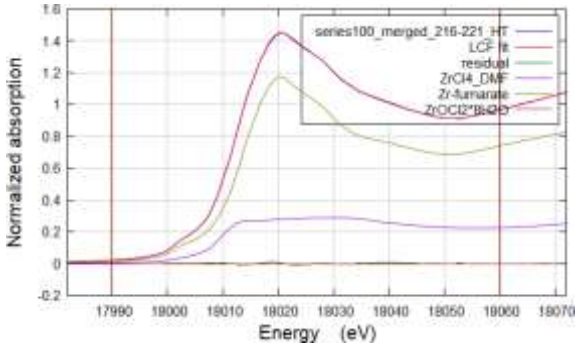
series100_merged_216-221_HT
LCF fit
residual
ZrCl4_DMF
Zr-fumarate
ZrOCl2*8H2O
Normalized absorption
Energy (eV)

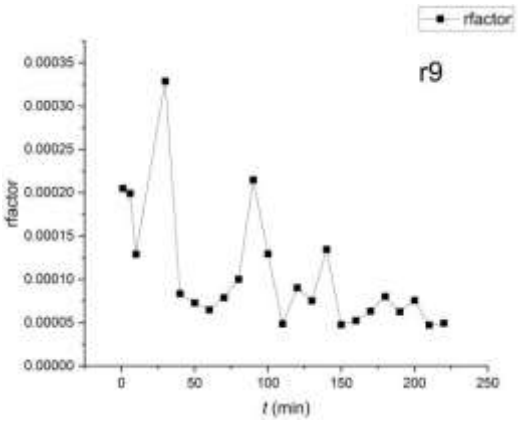

Fig. S4. Representative fits and *R*-factors of the LCFs. The fits were performed with three references: $ZrCl_4$-DMF, Zr-fumarate (Zr-oxocluster), and $ZrOCl_2 \cdot 8H_2O$ (Zr-tetramer). r8: comparison of the last reaction spectra to the two references clearly shows the difference in the fitting to the tetramer and the Zr-oxocluster.

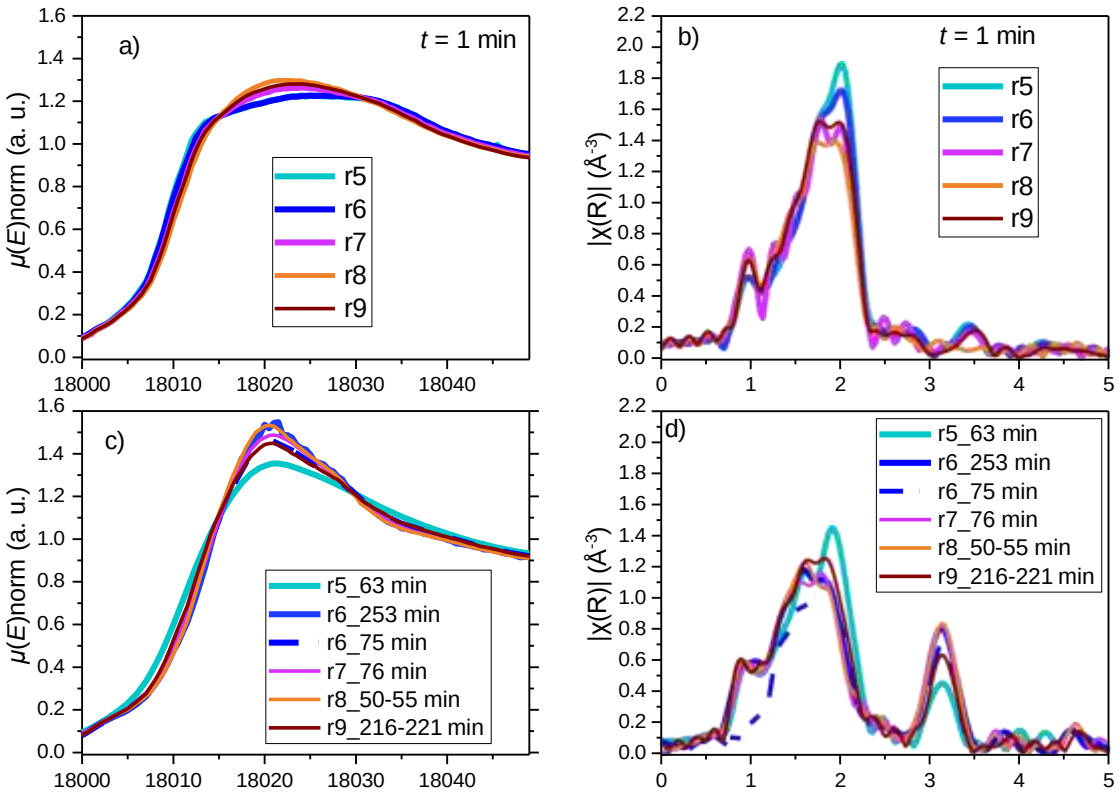

Fig. S5 XAS spectra for the kinetics series, reactions **r5-r9** with: a,b) the first registered spectra in XANES and EXAFS regions, respectively; c,d) the last registered spectra in XANES and EXAFS regions, and the curves for **r6** obtained after ca. 75 min.

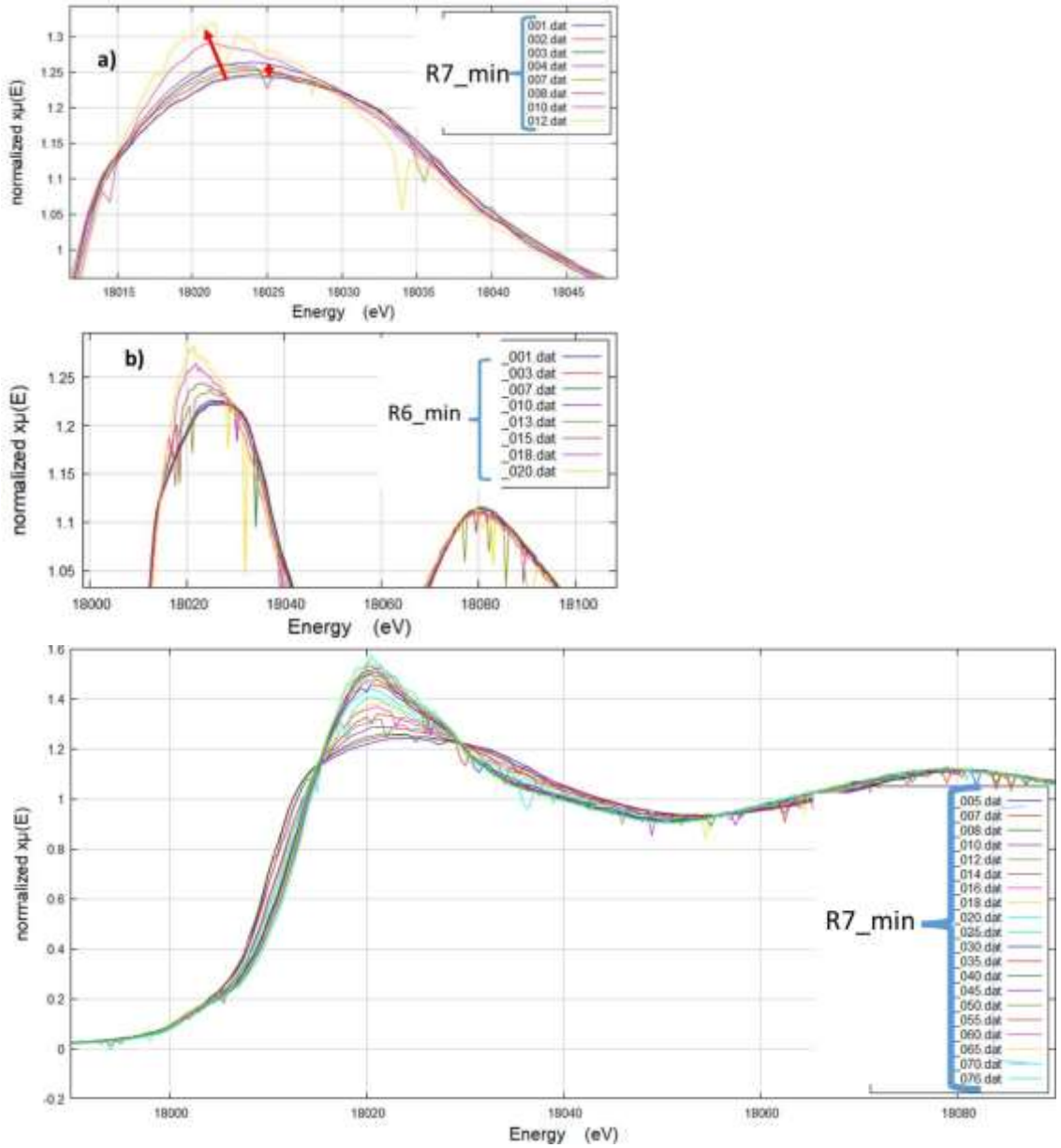

c)

Fig. S6 Selected in-situ XANES spectra for r7 and r6. The spectra were collected each minute and the numer corresponds to the minutes from data recording start. The spectra show at least two steps in r7 and moslty 1 step in r6. The lowest panel shows the spectral evolution of the r7.

5. LCF and reaction kinetics

The kinetic curves were obtained by fitting the three reference spectra: ZrCl4-DMF solution, Zr-fumarate and $ZrOCl_2 \cdot 8H_2O$ pellets. All weights were between 0 and 1 and their sum was constraint to one. Fits were carried out with free E_0.

5.1 Water series

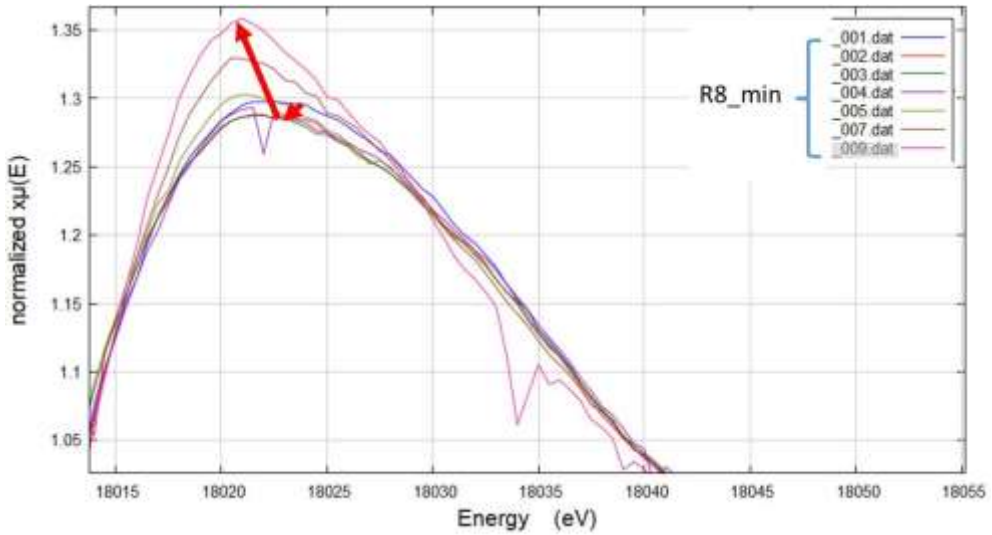

Fig. S7 Selected in-situ XANES spectra for **r8**. The spectra were collected each minute and the scan number corresponds to the minutes from the start of data recording. The spectra clearly shows at least two steps in the reaction (1-3 min, and 4 min - onwards).

5.2 Temperature series

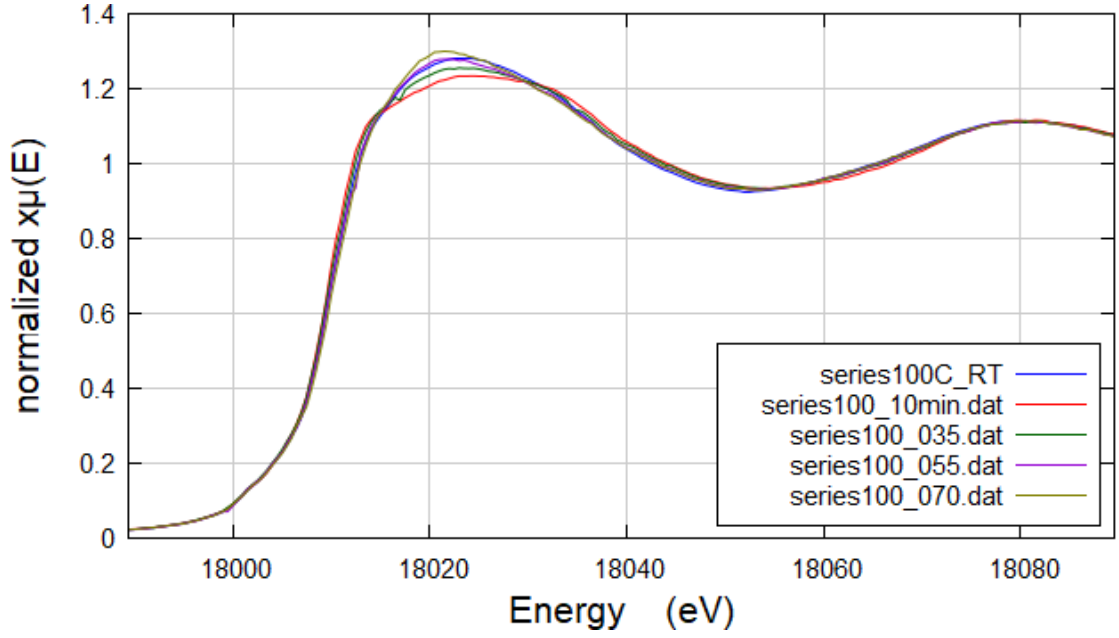

a)

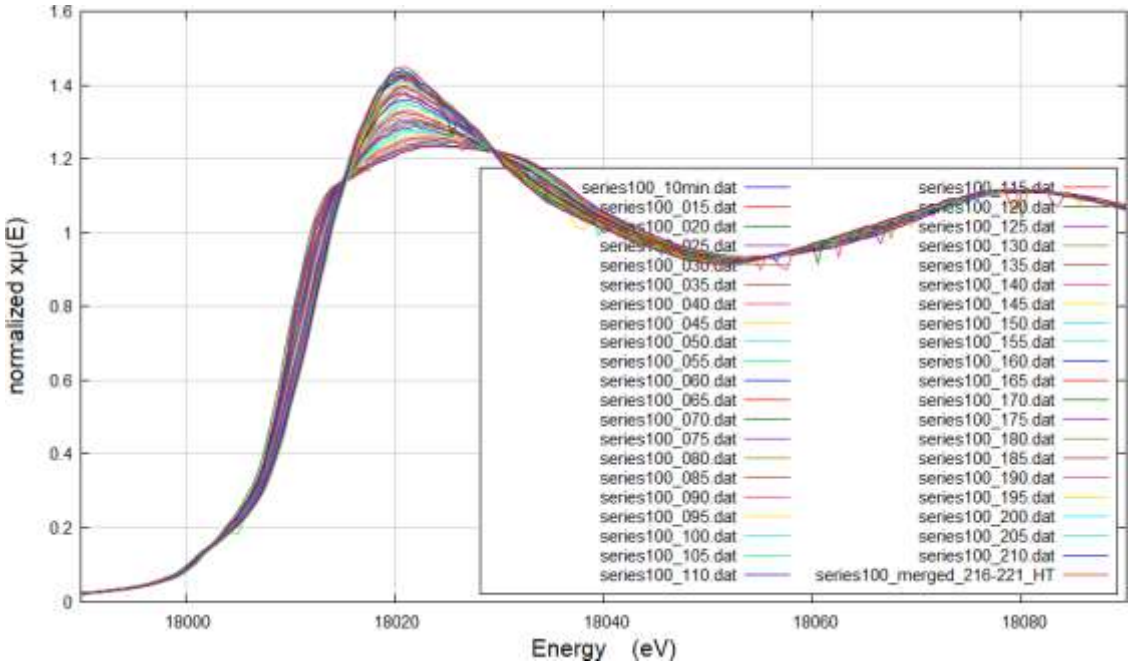

b)

Fig. S8 a) selected curves of the MOF-synthesis reaction **r9** that demonstrates the changes in the spectra of the solution at R*T*, 10 min into the fast ramp heating and the spectra obtained at 100 °C after 35-70 min; b) XANES region of the spectral series used to produce the kinetic curve with the first and last files as the two standards for linear combination fitting.

6. Characterization of MOFs formed in the in-situ reactions

6.1 Modulator series

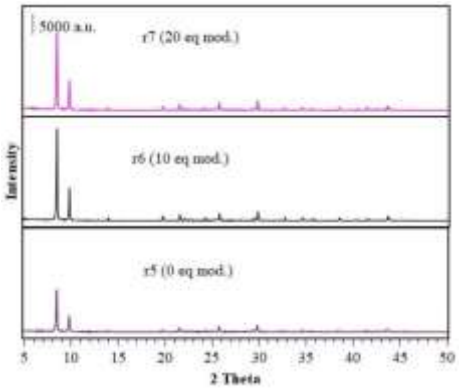

a)

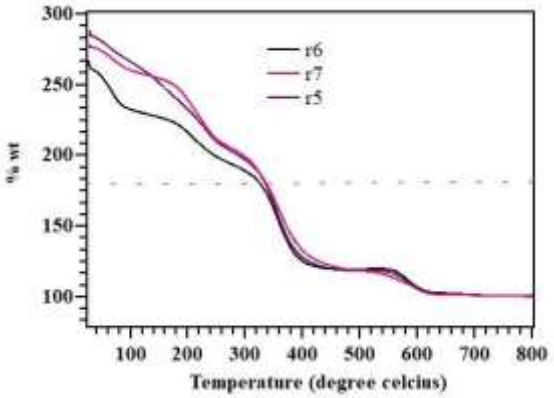

c)

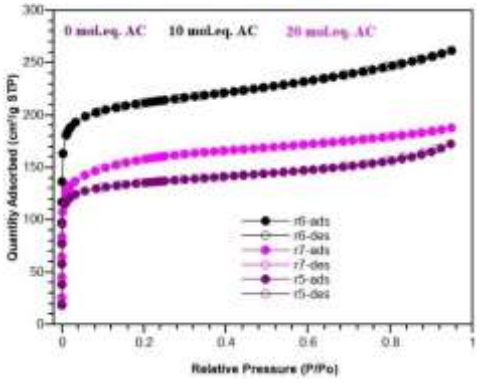

b)

Sample	Surface area (m2/g)	Pore volume at p/p0 = 0.94
r5 (0 mol eq.)	529	0.26
r6 (10 mol eq.)	826	0.40
r7(20 mol eq.)	590	0.28

Fig. S9 PXRD (a), BET (b), and TGA (c) characterization of the r5 – r7 reaction products.

The precipitates of the reactions were separated by centrifugation, washed, dried, and characterized with powder XRD, TGA, N_2 sorption at 77K, and Raman spectroscopy where possible. The XRD, TGA, and BET data on the modulator series are presented in Figure S6. All three samples are well crystalline with the diffraction pattern corresponding to that of Zr-fumarate. The sample synthesized without the modulator has a lower surface area, and slightly higher linker-to-metal ratio in the product than the one expected for the ideal Zr-Fumarate (TGA step for linker decomposition at 179.6 wt%).

The increase in intensity and appearance of well-defined sharp peaks in PXRD indicates the formation of larger crystallites. Such an effect has been previously observed with the addition of a modulator in the Zr-Fumarate synthesis.[4] In all the previous studies, the PXRD reported for synthesis without a modulator showed no reflection. However, we see the well-defined and expected reflection in the PXRD confirming the formation of Zr-Fumarate. The important difference between previously reported synthesis and our synthesis is the amount of DMF, our being highly concentrated.

The thermogravimetric analysis shows almost no difference in between the samples except the mass loss due to the removal of physiosorbed solvent. The dashed horizontal line indicates the expected weight loss for the ideal Zr-fumarate. The **r6** sample prepared with 10 eq. of the modulator shows a mass loss for linker decomposition closer to the theoretical mass loss for ideal MOF. The **r5** and **r7** showed mass loss larger than theoretically expected indicating the presence of unreacted organic linker residue.

All three samples were evaluated for porosity. The calculated BET surface area from the N_2 sorption at 77K are shown in the table. MOF made with 10 eq. of the modulator showed the highest surface area (826 m^2/g). The Wißmann et al.[4] has reported a surface area 856 m^2/g for Zr-fumarate made with 30 eq. of the modulator.

6.2 Temperature series

The PXRD patterns of the samples synthesized at 100, 120, and 130 °C with 20 eqv. modulator are shown in figure 8a. All the patterns show the diffraction peaks expected for Zr-fumarate indicating the successful formation of Zr-Fumarate MOF. A minor difference in the intensity of the diffraction peaks (at low angle) was noticed going from low temperature to high temperature. Intensity increases at higher temperatures. However, this increase is not as significant as one noticed with an increase in modulator amount. The TGA analysis also shows an almost similar weight loss profile for three samples. However, the N_2 sorption at 77K shows the difference in the N_2 uptake, and hence the surface area and pore volume. The sample prepared at a low temperature (100) showed a lower surface area while the sample prepared at 130 C showed high surface area.

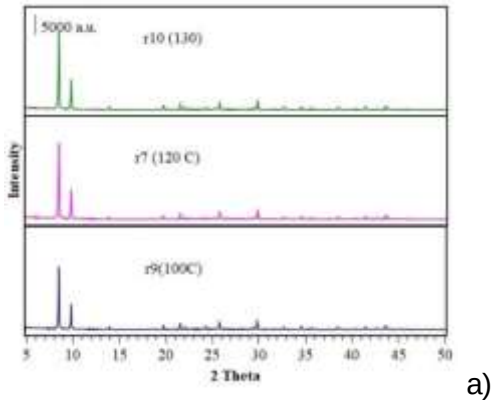

a)

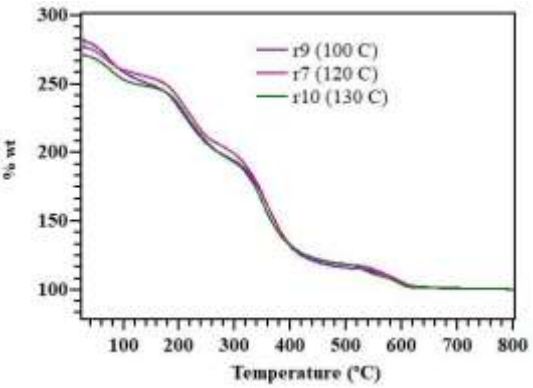

c)

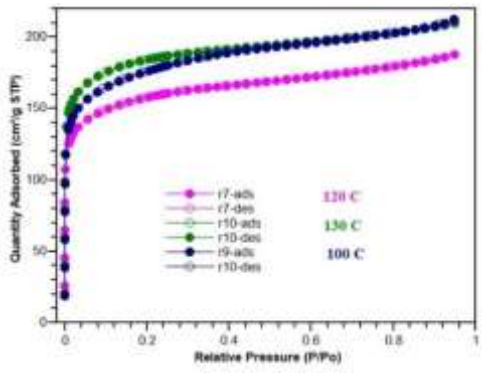

b)

Sample	Surface area (m^2/g)	Pore volume at p/p^0 = 0.94
r9 (100° C)	652	0.32
r7 (120° C)	590	0.28
r10(130° C)	693	0.32

Fig. S10 PXRD (a), BET (b), and TGA (c) characterization of the **r7, r9, r10** reaction products.

6.3 Water series

In the absence of water, we did not see any precipitate formation in the reaction tube. The reaction solution was as clear as the initial reaction mixture. The addition of 3 molar eq. water led to the successful formation of MOF. Excess amounts of water (8 molar eq.) in the synthesis also gave the Zr-Fumarate MOF product. The laboratory PXRD did not show much difference between the products. However, differences were observed in the TGA and porosity analysis. MOF sample prepared with excess water (**r8**) showed continued mass loss with heating from

RT up to 300C while the Zr-fumarate prepared with 3 eq. showed a two-step mass loss. The sample prepared with an excess of water showed lower N_2 uptake almost half compared to MOF prepared with only 3 eq. of water.

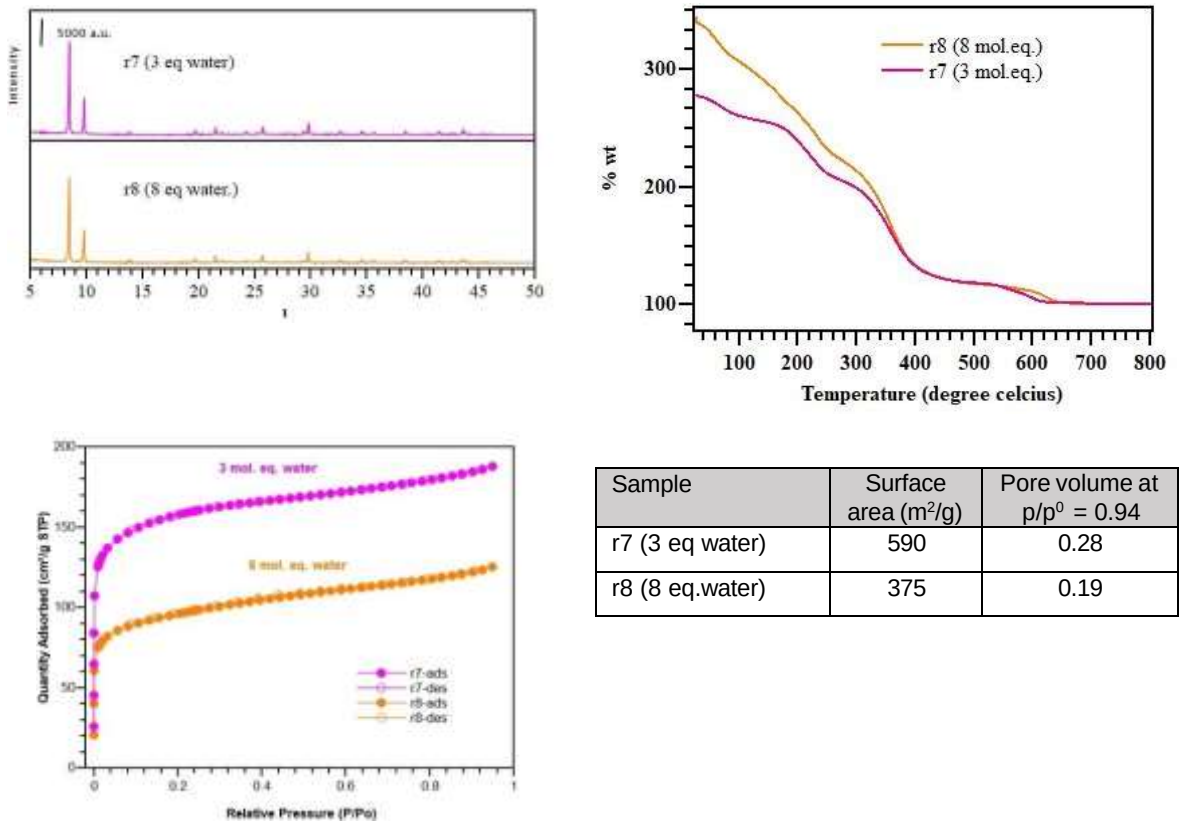

Sample	Surface area (m^2/g)	Pore volume at p/p^0 = 0.94
r7 (3 eq water)	590	0.28
r8 (8 eq.water)	375	0.19

Fig. S11. Comparison of the PXRD (a), BET (b), and TGA (c) characterization of the **r7, and r8** reaction products.

6.4 Analysis of the Raman spectra

Raman spectra of the dried reaction products are shown on the figure 8, and the peak assignment is collected in the Table 4. The assignment is based on literature data and the assumptions that symmetric modes are most intense in the Raman spectra.[5-9] Fumaric acid has a set of fundamental Raman-active skeletal vibrations at 3069 (w, ν_s(CH)) – 1685 (vs, ν_s(C=O)) – 1605 (w, ν(C=C)) – 1437 (w, δ(COH)) - 1298 (s, δ(CCH)) – 972 (w) and 913 (m, γ(CCH)) – 693 (m, γ(CCOO)) – 449 (vw, γ(COH)), and 199 (m, δ(CCC)) cm^{-1}.[5]

The Raman features of the linker skeletal modes (<1800 cm^{-1}) are usually altered when hydrogen in the −COOH group is replaced by a cation, allowing in some cases for distinguishing between different coordination of the linker to a cation.[6] In Zr-fumarate, the linker is coordinated via two oxygen atoms of the carboxylate group in *syn, syn* coordination changing the C=O mode to symmetric and asymmetric COO^- stretching. The most intense peak at 1662 cm^{-1} is assigned to C-O stretching of the coordinated linker. The blue shift with respect to fumaric acid can be explained by larger positive charge on the ion resulting to coordination to the clusters. The peaks at 1424 - 1437 cm^{-1} can comprise the combination of $\nu_s(COO^-)$ with bending modes of $-CH_2$ and -COH.

Table S3. Raman features in 200 – 1800 cm^{-1} region of MOF products obtained in the reactions r**5** - r**10**

Raman shift, cm^{-1}	**Compound**	**Assignment (main contribution)**
3060 m*	fumarate	ν(C-H)
2940 m	fumarate	ν(C-H)
1662 vs	fumarate	$\nu_{as}(COO^-)$
1590-1542 w, br	fumarate	ν(C=C)
1437-1424 vs	fumarate	$\nu_s(COO^-)$ [7]
1275 s	fumarate	δ(CCH)
1103 w	fumarate	δ(CCH)
995 w	fumarate	δ(CCO)
902 m	fumarate	ν_s(C-C)
863 m	fumarate	ν_{as}(C-C)
758 m	fumarate	Zr-O-C (linker)
664 m	fumarate	γ(CCOO)
501 m	cluster	ν_s (Zr−μ_3−O)
408 w	cluster	Zr-O
370 w	cluster	ν_{as} (Zr−μ_3−O)
304 w	fumarate	
249 w	fumarate	δ(CCC)

Assignment as discussed in the text.
*Intensities are indicated as: br – broad, vs – very strong, s – strong, m – medium, w – weak

There are two types of Zr-O bonds in MOF-801: 1) those of the cluster, Zr−μ_3−O and 2) Zr-O-C of cluster – linker coordination. This first group was observed at 493 and 210 cm^{-1}, for ν_s, and ν_{as}, respectively, in Zr-UiO-66.[10] We suggest that the peak at 501 cm cm^{-1} and possibly 408, 370 is(are) responsible for this bond in our data. For the Zr-O-C bond, we tentatively suggest the one at 758 cm could be related to linker-cluster coordination.

In addition to the main modes identified and summarised in the Table 3, a group of modes at 2970-1317-1297-953-889-695 cm^{-1} with visible intensity correlation between the samples, marked with asterisks on the spectra, might be noticed. The intensity of this group of peaks increases in the order: r8 < r7/r5 < r9 < r6 < r10, which shows a straightforward negative correlation with the surface area of the samples. Thus, these peaks should be related to impurities in the pores and/or defects degrading the SSA of MOFs. The set of these vibrations is very close to that of the fumaric acid powder, except a strong peak at 1682 cm^{-1} that is hindered by the main vibration of the fumarate linker. These peaks can thus be assigned to the unreacted linker in the pores. Presence of DMF and acetic acid in the pores / MOF structure was found by Ragon et al.[11, 12]

Table S4. Comparison of the observed extra peaks in the Raman spectra of in-situ generated MOFs and reference compounds

The unknown compound, this work, cm^{-1}	Acetic acid,[13] pure	Me(Acac) (Me = Na, K, Ni, Co), solid, aqueous, hydrated [14]	DMF,[1] liquid	Assignment
3028, m	3020	3013 - 3030	2934, s	C-H stretching in $-CH_3$
2970, s	2937, s, shoulders at 2985,	2925 - 2941	2861, s	
obscured ~1700 (?)	1664, m		1661, m	ν(C=O), $\nu_{as}(COO^-)$

[1] https://www.chemicalbook.com/SpectrumEN_68-12-2_IR1.htm

		1512 – 1575		$v_{as}(COO^{-})$
~1460, m	1428, m	1402 – 1456 (2 modes)	1441 1408	$v_{s}(COO^{-})$
1317, m	1366, w	1340 – 1357 (1 mode)		
1297, s				monodentate acetate groups
1020, m	1014, w	1009 – 1070 (2 modes)	1096, m	
953, m		924 – 962 (1 mode)		v(C-C)
889, s	893, intense, sharp		867, intense, sharp	v(C-C)
695, m	621, m, sharp	615 – 680 (two modes)	660, intense, sharp	
	446, w, sharp		407, m 319, mw	

References

(1) Mak, T. C. W. Refinement of the crystal structure of zirconyl chloride octahydrate. *Canadian Journal of Chemistry* **1968**, *46* (22), 3491-3497. DOI: 10.1139/v68-579.
(2) Ravel, B.; Newville, M. ATHENA, ARTEMIS, HEPHAESTUS: data analysis for X-ray absorption spectroscopy using IFEFFIT. *Journal of Synchrotron Radiation* **2005**, *12* (4), 537-541. DOI: doi:10.1107/S0909049505012719.
(3) Furukawa, H.; Gándara, F.; Zhang, Y.-B.; Jiang, J.; Queen, W. L.; Hudson, M. R.; Yaghi, O. M. Water Adsorption in Porous Metal–Organic Frameworks and Related Materials. *Journal of the American Chemical Society* **2014**, *136* (11), 4369-4381. DOI: 10.1021/ja500330a.
(4) Wißmann, G.; Schaate, A.; Lilienthal, S.; Bremer, I.; Schneider, A. M.; Behrens, P. Modulated synthesis of Zr-fumarate MOF. *Microporous and Mesoporous Materials* **2012**, *152*, 64-70. DOI: https://doi.org/10.1016/j.micromeso.2011.12.010.
(5) Bayer, M. C.; Jessen, C.; Kornath, A. J. Preparation and Characterization of Protonated Fumaric Acid. *Zeitschrift für anorganische und allgemeine Chemie* **2020**, *646* (7), 333-339. DOI: https://doi.org/10.1002/zaac.202000091.
(6) Hadjiivanov, K. I.; Panayotov, D. A.; Mihaylov, M. Y.; Ivanova, E. Z.; Chakarova, K. K.; Andonova, S. M.; Drenchev, N. L. Power of Infrared and Raman Spectroscopies to Characterize Metal-Organic Frameworks and Investigate Their Interaction with Guest Molecules. *Chemical Reviews* **2021**, *121* (3), 1286-1424. DOI: 10.1021/acs.chemrev.0c00487.
(7) De Gelder, J.; De Gussem, K.; Vandenabeele, P.; Moens, L. Reference database of Raman spectra of biological molecules. *Journal of Raman Spectroscopy* **2007**, *38* (9), 1133-1147. DOI: 10.1002/jrs.1734.
(8) Iancu, S. D.; Stefancu, A.; Moisoiu, V.; Leopold, L. F.; Leopold, N. The role of Ag+, Ca2+, Pb2+ and Al3+ adions in the SERS turn-on effect of anionic analytes. *Beilstein Journal of Nanotechnology* **2019**, *10*, 2338-2345. DOI: 10.3762/bjnano.10.224.
(9) Ganesh, M.; Hemalatha, P.; Peng, M. M.; Cha, W. S.; Jang, H. T. Zr-Fumarate MOF a Novel CO2-Adsorbing Material: Synthesis and Characterization. *AEROSOL AND AIR QUALITY RESEARCH* **2014**, *14* (6), 1605-1612. DOI: 10.4209/aaqr.2013.11.0337.
(10) Shearer, G. C.; Chavan, S.; Ethiraj, J.; Vitillo, J. G.; Svelle, S.; Olsbye, U.; Lamberti, C.; Bordiga, S.; Lillerud, K. P. Tuned to Perfection: Ironing Out the Defects in Metal-Organic Framework UiO-66. *Chemistry of Materials* **2014**, *26* (14), 4068-4071. DOI: 10.1021/cm501859p.
(11) Ragon, F.; Chevreau, H.; Devic, T.; Serre, C.; Horcajada, P. Impact of the Nature of the Organic Spacer on the Crystallization Kinetics of UiO-66(Zr)-Type MOFs. *CHEMISTRY-A EUROPEAN JOURNAL* **2015**, *21* (19), 7135-7143. DOI: 10.1002/chem.201406119.
(12) Ragon, F.; Horcajada, P.; Chevreau, H.; Hwang, Y. K.; Lee, U. H.; Miller, S. R.; Devic, T.; Chang, J.-S.; Serre, C. In Situ Energy-Dispersive X-ray Diffraction for the Synthesis Optimization and Scale-up of the Porous Zirconium Terephthalate UiO-66. *Inorg. Chem.* **2014**, *53* (5), 2491-2500. DOI: 10.1021/ic402514n.
(13) Wan, F.; Du, L.; Chen, W.; Wang, P.; Wang, J.; Shi, H. A Novel Method to Directly Analyze Dissolved Acetic Acid in Transformer Oil without Extraction Using Raman Spectroscopy. *Energies* **2017**, *10* (7), 967.
(14) Frost, R. L.; Kloprogge, J. T. Raman spectroscopy of the acetates of sodium, potassium and magnesium at liquid nitrogen temperature. *Journal of Molecular Structure* **2000**, *526* (1), 131-141. DOI: https://doi.org/10.1016/S0022-2860(00)00460-9.